A combined crossed-beam, *ab initio*, and Rice–Ramsperger–Kassel–Marcus investigation of the reaction of carbon atoms $C(^3P_j)$ with benzene, $C_6H_6(X^1A_{1g})$ and d_6-benzene, $C_6D_6(X^1A_{1g})$

I. Hahndorf, Y. T. Lee, and R. I. Kaiser[a)]
Institute of Atomic and Molecular Sciences, 107 Taipei, Taiwan, Republic of China

L. Vereecken[b)] and J. Peeters
Department of Chemistry, Celestijnenlaan 200F, B-3001 Heverlee, Belgium

H. F. Bettinger[c)]
Lehrstuhl für Organische Chemie II, Ruhr-Universität Bochum, Germany

P. R. Schreiner and P. v. R. Schleyer[d)]
Department of Chemistry, University of Georgia, Athens, Georgia 30602

W. D. Allen and H. F. Schaefer III
Center for Computational Quantum Chemistry, University of Georgia, Athens, Georgia 30602

(Received 22 March 2001; accepted 26 September 2001)

The reactions of atomic carbon, $C(^3P_j)$, with benzene, $C_6H_6(X^1A_{1g})$, and with d_6-benzene, $C_6D_6(X^1A_{1g})$ were investigated at twelve collision energies between 8.8 and 52.5 kJ mol^{-1} using the crossed molecular beams technique. Forward-convolution fitting of the data, high-level electronic structure calculations, and Rice–Ramsperger–Kassel–Marcus (RRKM) investigations on the singlet and triplet C_7H_6/C_7D_6 potential energy hyperface suggest that at low collision energies the chemical reaction dynamics are indirect and dominated by large impact parameters. As the collision energy increases, smaller impact parameters become more important, and the chemical dynamics is increasingly direct. At all collision energies, the reaction proceeds on the triplet surface via a barrierless addition of the carbon atom to form a bicyclic intermediate followed by ring opening of the initial collision complex to a seven-membered ring intermediate (cycloheptatrienylidene). The latter decomposes without exit barrier to the thermodynamically less stable 1,2-didehydrocycloheptatrienyl radical, $C_7H_5(X^2B_1)+H$, and its deuterated $C_7D_5(X^2B_1)+D$ counterpart. The formation of a C_7D_6 adduct is observed as a second channel. The barrierless route for the destruction of benzene can help to model important pathways for the synthesis of higher polycyclic aromatic hydrocarbon derivatives in the interstellar medium, in outflows of dying carbon stars, in hydrocarbon-rich planetary atmospheres, as well as in oxygen-poor combustion flames. © *2002 American Institute of Physics.* [DOI: 10.1063/1.1418744]

I. INTRODUCTION

Unraveling the elementary reactions of benzene, the very first ''building block'' of polycyclic aromatic hydrocarbons (PAHs), is essential to understand the formation and fate of complex PAHs in various astrochemical and terrestrial environments. Particular attention has been devoted to circumstellar envelopes of carbon stars,[1] hydrocarbon-rich planetary atmospheres,[2] combustion processes,[3] and environmental science. Benzene has been detected in oxygen-poor methane, ethane, ethylene, propane, and n-butane flames,[4] and has been suggested to be the initial aromatic molecule involved in the formation of PAHs and of soot.[5] Since both PAHs and soot particles are carcinogenic, these species represent significant atmospheric pollutants and pose a considerable health hazard.[6] The very first detection of benzene outside our solar system was announced only recently.[7] Cernicharo *et al.* reported this discovery by the *Infrared Space Observatory* (ISO) towards the proto planetary nebula CRL 618, i.e., an object in the evolutionary stage between carbon-rich asymptotic giant branch (AGB) stars and a planetary nebula.

All reaction networks which model the formation of PAHs in the interstellar medium and in combustion flames agree that the benzene molecule is one of the key reaction intermediates in the synthetic sequences via multiple reaction chains.[8] Benzene may also be involved in the production of fullerenes and carbon nanotubes.[9] However, the elementary reactions of benzene itself are poorly understood. Studies of the reactive collisions of C_6H_6 with the cyano radical, $CN(X^2\Sigma^+)$,[10] and with ground-state atomic oxygen, $O(^3P_j)$[11] employing the crossed molecular beam technique have been reported. Both processes were found to proceed

[a)]Also at Department of Physics, University Chemnitz, 09107 Chemnitz, Germany. Present address: Department of Chemistry, University of York, York YO10 5DD, UK. Electronic mail: rik1@york.ac.uk
[b)]Electronic mail: Luc.Vereecken@chem.kuleuven.ac.be
[c)]Electronic mail: Holger.Bettinger@ruhr-uni-bochum.de
[d)]Also at Institut für Organische Chemie, Universität Erlangen-Nürnberg, Henkestrasse 42, 91052 Erlangen, Germany.

TABLE I. Experimental beam conditions and 1σ errors: most probable velocity of the carbon beam $v_p(C)$, most probable velocity of the benzene beam $v_p(b)$, speed ratio of the carbon beam $S(C)$, speed ratio of the benzene beam, $S(b)$, most probable collision energy, E_c, and center-of-mass angle, θ_{CM}.

Reaction	$v_p(C)$, m s^{-1}	$v_p(b)$, m s^{-1}	$S(C)$	$S(b)$	E_c, kJ mol^{-1}	θ_{CM}, °
$C+C_6D_6$	1220±10	440±15	5.9	17.2	8.8±0.2	68.4±0.9
$C+C_6D_6$	1925±25	640±10	7.8	12.8	21.4±0.6	66.7±0.6
$C+C_6D_6$	2350±63	770±10	8.1	12.7	32.1±1.6	66.4±0.8
$C+C_6D_6$	2780±90	780±15	4.4	12.7	43.7±2.7	63.0±1.2
$C+C_6D_6$	3067±8	770±10	5.7	12.7	52.5±0.3	60.4±0.4
$C+C_6H_6$	1280±30	420±10	4.5	14.0	9.4±0.9	64.9±0.6
$C+C_6H_6$	1745±40	482±10	8.7	12.5	17.0±0.8	60.8±1.0
$C+C_6H_6$	1950±20	635±5	7.7	12.3	21.8±1.1	64.7±0.4
$C+C_6H_6$	2180±30	640±10	6.2	12.3	26.9±1.6	62.3±0.7
$C+C_6H_6$	2540±20	780±10	4.2	12.8	36.7±1.5	63.4±0.5
$C+C_6H_6$	2700±40	780±10	5.4	12.8	41.1±1.1	62.0±0.7
$C+C_6H_6$	3012±18	780±10	6.4	12.8	50.3±0.7	59.3±0.5

via an initial attack of the benzene ring forming C_6H_6CN and C_6H_6O adducts, respectively. The addition of the cyano radical proceeds barrierless, whereas the oxygen atom reaction involves a barrier of 16–22 kJ mol^{-1}. Both initial complexes undergo subsequent H-atom elimination to form cyanobenzene, C_6H_5CN, and the phenoxy radical, C_6H_5O, respectively. Formation of a phenol adduct was identified as a minor pathway and suggested to proceed via intersystem crossing (ISC) of the initial collision complex and hydrogen migration. Therefore, both reactions conserve the benzene ring and do not destroy the aromatic 6π–electron system. Previous studies of the related reaction of atomic carbon with benzene were restricted to bulk experiments such as the reactions of suprathermal ^{11}C recoil atoms with liquid benzene at 293 K[12] and arc-generated carbon atoms with solid benzene at 77 K.[13] It was suggested that ^{11}C adds to the π–electron system followed by ring opening and reaction with a second benzene molecule to a cycloheptatriene derivative. In addition, ^{11}C was found to insert into a C–H bond to give the phenylcarbene intermediate. The latter reacted with C_6H_6 to give diphenylmethane. Contrary to these hot atom experiments,[12] Shevlin *et al.* suggested solely an insertion process into a C–H bond of benzene.[13] However, these investigations were performed under bulk conditions, and no information about the nascent product distribution is available. In addition, neither the electronic states of the reacting carbon atoms nor their kinetic energy is known; hence, only conjectures rather than detailed mechanistic conclusions are possible. Third, such reactive intermediates can undergo secondary reactions, which complicate assignment of the nascent reaction products.

We now present a complete investigation of the elementary reaction of atomic carbon, $C(^3P_j)$, with benzene, $C_6H_6(X\,^1A_{1g})$, and with perdeutero benzene, $C_6D_6(X\,^1A_{1g})$, under single collision conditions utilizing the crossed beam approach. Compared to our more limited study of this important reaction,[14] the present paper investigates the collision energy-dependent triply differential cross sections and the underlying dynamics at twelve collision energies. These experimental findings are discussed in the light of previous[15] and new electronic structure calculations and are compared to a microvariational treatment of the reactions which predicts branching ratios as well as the lifetime of the decomposing complex(es).

II. EXPERIMENT

All experiments were performed with the 35″ crossed molecular beams machine described in detail earlier.[16] Briefly, a pulsed supersonic carbon beam was generated via laser ablation of graphite at 266 nm.[17] The 30 Hz, 35–45 mJ output of a Spectra Physics GCR-270-30 Nd: YAG laser was focused onto a rotating carbon rod, and the ablated species were seeded into a pulse of neat helium gas at 4 atm backing pressure. A four-slot chopper wheel mounted after the ablation zone selected a 9.0 μs segment of the seeded carbon beam. Table I compiles the experimental beam conditions and uncertainties. This carbon beam crossed a second pulsed beam of benzene at 90° in the interaction region of the scattering chamber. Benzene was either seeded (neon, argon) or antiseeded (krypton, xenon) in the carrier gas. We were unable to perform reactions with benzene seeded in helium, as the center-of-mass angle of this system is too close to the secondary beam and hence outside the reach of our detector. If we choose the very fast part of the benzene beam, the reaction of benzene and noble-gas-benzene-clusters can be eliminated. Reactively scattered products were detected in the plane defined by the two beams using a rotatable detector consisting of a Brink-type electron-impact ionizer,[18] quadrupole mass filter, and a Daly ion detector at various laboratory angles. The velocity distribution of the products was recorded in time-of-flight (TOF) mode accumulating between 5 and 120 min at each angle. Information on the chemical reaction dynamics was gained by fitting the TOF spectra and the product angular distribution in the laboratory frame (LAB) using a forward-convolution routine.[19] This procedure assumes an angular flux distribution $T(\theta)$ and the translational energy flux distribution $P(E_T)$ in the center-of-mass system (CM), which are separable. Laboratory TOF spectra and the laboratory angular distributions were then calculated from these $T(\theta)$ and $P(E_T)$ averaged over the apparatus and beam functions. Best TOF and laboratory angular distributions were achieved by refining adjustable $T(\theta)$ and $P(E_T)$ parameters.

III. ELECTRONIC STRUCTURE CALCULATIONS

Becke's[20] three-parameter hybrid Hartree–Fock functional was employed in this study in conjunction with the correlation functional of Lee, Yang, and Parr (B3LYP).[21] The 6-31G* basis set was used for geometry optimizations and for analytic second-derivative computations. The latter characterized the stationary points as minima or saddle points on the PES. The relative energies were corrected by unscaled harmonic zero-point vibrational energies (ZPVE). Subsequently, the 6-311+G** basis set was utilized to reoptimize the geometries. All energies given in the text were obtained at the B3LYP/6-311+G**+ZPVE(B3LYP/6-31G*) level of theory except if noted otherwise. The barrier for the cleavage of an H_2 molecule from C_7H_6 isomer cyclohepta-1-yne-3,5-diene was refined by G2(B3LYP/MP2) theory, a modification of the G2(MP2) approach of Curtiss *et al.*[22] introduced by Bauschlicher and Partridge.[23] In addition, we employed a multiconfiguration self-consistent field wave function of the complete active space type (CASSCF) for the description of cyclohepta-1,2,4,6-tetraene-1,3-diyl. The active space consisted of ten electrons in ten molecular orbitals. These were the seven π/π^* and the three σ-allyl type in-plane MOs. The standard density functional theory (DFT) integration grids and convergence criteria of the GAUSSIAN 98 program were used throughout.[24] In the entrance channel, i.e., the initial approach of the carbon atom to the benzene molecule, we located a minimum on the seam of crossing (MSX) between the singlet ($^1A'$) and triplet ($^3A''$) PES using a state-averaged CASSCF wave function. The algorithm for locating the MSX has been described by Bearpark *et al.*[25] and is implemented in the GAUSSIAN program. The active space for the MSX computation consisted of six electrons distributed over six molecular orbitals. The initial orbitals were selected from a restricted open-shell Hartree–Fock computation (ROHF/6-31G*) at the B3LYP/6-311+G** geometry of the initial addition product. At the MSX geometry, we computed the norm of the spin–orbit coupling matrix element between the lowest singlet and triplet states using the one-electron approximation to the full Breit–Pauli Hamiltonian. Two electron effects are approximately accounted for by using the effective nuclear charges suggested by Koseki *et al.*[26]

IV. RRKM—MASTER EQUATION ANALYSIS

The collision energy and pressure-dependent product distributions of the reaction of benzene with atomic carbon were obtained by an RRKM-master equation (RRKM-ME) analysis. This was based on the triplet C_7H_6 potential energy surface published earlier by Bettinger *et al.*[15] For reasons explained below, we used the experimental value for the energy of the dissociation limit to form the 1,2-didehydrocycloheptatrienyl radical rather than the theoretical value. The methodology used for the RRKM-ME analysis has been discussed in detail before.[27] Briefly, the energy-specific rate constants $k(E)$ for each of the unimolecular reaction steps in the system are calculated by standard RRKM theory;[28] the barrierless reaction to 1,2-didehydrocycloheptatrienyl is treated microvariationally, where the rate constant $k(E)$ is optimized by minimizing the sum of states along the reaction path using a detailed B3LYP-DFT/6-31G(d) characterization of the energy profile and vibrational wave numbers as a function of the reaction coordinate.[29] Due to numerical difficulties in the quantum-chemical characterization of the vibrational modes of the entrance channel to the initial addition product, we can only estimate this transition state's wave numbers based on the results of our DFT calculations. As a consequence, we are also unable at this time to calculate reliable absolute overall rate constants. Due to the absence of an energy barrier in the initial association pathway, we expect a high rate constant $k \sim 10^{-10}\,\mathrm{cm^3\,s^{-1}}$ with a slight negative temperature dependence, since the transition state tightens at higher energies and because of increased redissociation rates leading to regeneration of the reactants from the C_7H_6 intermediates. The initial energy distribution function of the C_7H_6 intermediates as formed in the $C_6H_6+C(^3P_j)$ reactions was obtained from detailed balance considerations based on the RRKM formalism, assuming thermal energy distributions for the initial reactants. Energy transfer processes in molecular collisions, needed for prediction at higher pressures, were modeled using Troe's biexponential model.[30] The overall product distribution as function of collision energy and pressure is then obtained by a master equation analysis based on a stochastic description of the reaction processes as implemented in our general purpose URESAM-3 kinetics computer program suite, using a small energy grain size of 1 $\mathrm{kJ\,mol^{-1}}$. Given the approximations needed for the entrance transition state, we report in the remainder of this section only on the effective product distribution and lifetime of the decomposing complex(es), in which redissociation to both reactants has been factored out.

RRKM-ME calculations for the reaction conditions as found in the crossed-beam experiments would require the knowledge of the distribution of the collision energy over the rotational or vibrational degrees of freedom of the adduct formed, so that the energy-specific data, as described in the RRKM calculations, can be applied to the relevant population. Unfortunately, these initial distributions depend on the exact reaction dynamics as a function of available energy, impact parameters, and relative orientation of the molecules. While some qualitative trends can be deduced, it is at present not possible to quantify the required distributions. Due to the lack of accurate nascent distributions for use as input data, it was decided to perform the calculations for thermal reaction conditions, for which the distributions can be calculated, and which apply to most realistic reaction conditions excluding direct reactions.

V. EXPERIMENTAL RESULTS

A. Reactive scattering signal

Reactive scattering signals were observed at mass to charge ratios $m/e = 89-84$ ($C_7H_5^+$ to C_7^+; benzene systems) and $94-84$ ($C_7D_5^+$ to C_7^+; perdeutero benzene experiments) at collision energies between 8.8 and 52.5 $\mathrm{kJ\,mol^{-1}}$. TOF spectra taken at lower m/e data for selected angles depict identical patterns and could be fit with the same center-of-

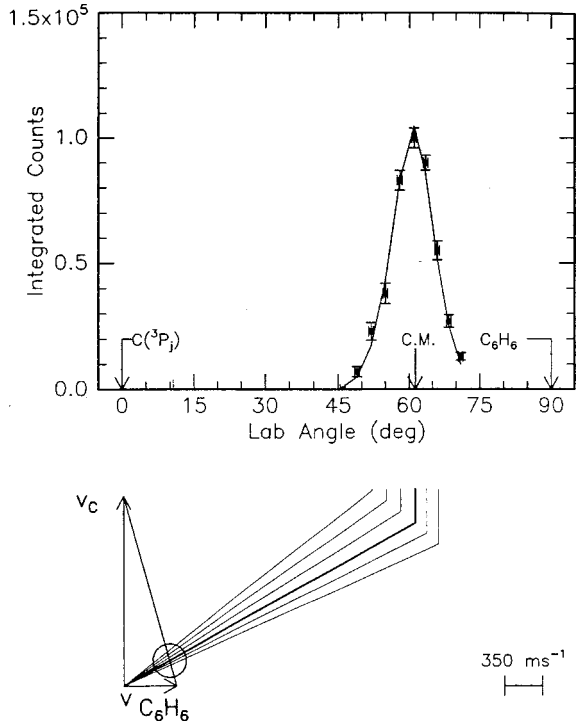

FIG. 1. Lower: Newton diagram for the reaction $C(^3P_j)+C_6H_6(X\,^1A_{1g})\rightarrow C_7H_5+H(^2S_{1/2})$ at a collision energy of 17.0 kJ mol^{-1}. The circle stands for the maximum center-of-mass recoil velocity of the 1,2-didehydrocycloheptatrienyl product assuming all the available energy is released as translational energy. Upper: Laboratory angular distribution of the C_7H_5 product. Circles and error bars indicate experimental data, the solid line the best fit distribution.

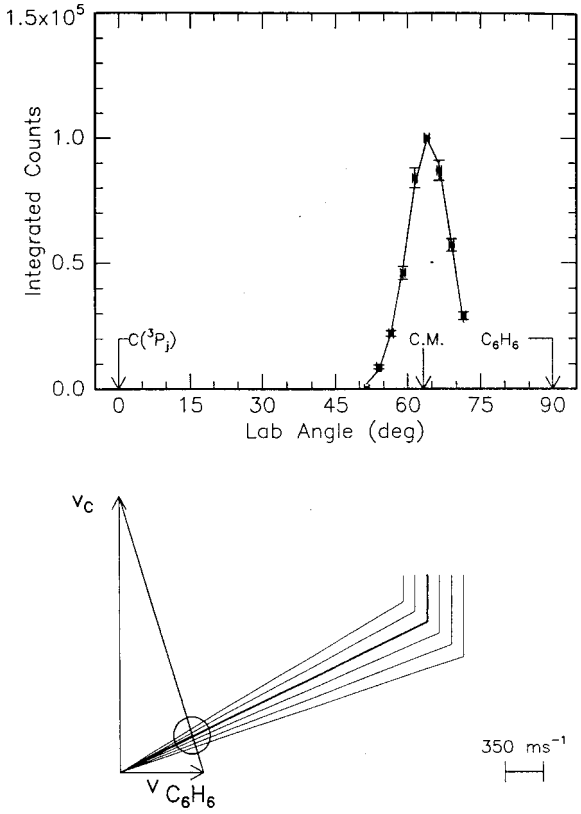

FIG. 2. Lower: Newton diagram for the reaction $C(^3P_j)+C_6H_6(X\,^1A_{1g})\rightarrow C_7H_5+H(^2S_{1/2})$ at a collision energy of 36.7 kJ mol^{-1}. The circle stands for the maximum center-of-mass recoil velocity of the 1,2-didehydrocycloheptatrienyl product assuming all the available energy is released as translational energy. Upper: Laboratory angular distribution of the C_7H_5 product. Circles and error bars indicate experimental data, the solid line the best fit distribution.

mass functions. This suggests that the signal at lower m/e ratios originates from cracking of the parent ion in the electron impact ionizer, and that only the carbon versus deuterium/hydrogen exchange channel exists. Hence, TOF spectra were taken at the most intense fragments $m/e=89$ $[C(^3P_j)+C_6H_6$ experiments] and $m/e=94$ $[C(^3P_j)+C_6D_6$ experiments]; selected data for a low, a medium, and the highest collision energies of the $C(^3P_j)/C_6H_6$ system are shown in Figs. 1–6; all remaining data are compiled in the Electronic Physics Auxiliary Publication Service (EPAPS) database of the American Institute of Physics.[31]

In addition, we investigated the formation of C_7H_6 and C_7D_6 adducts by recording TOF spectra at $m/e=90$ and 96, respectively, at selected collision energies of 21.6 and 21.4 kJ mol^{-1}. Averaging over a total data accumulation time of up to 24 h at each angle, the only signal we identified at $m/e=90$ resulted from $^{13}C^{12}C_6H_5^+$ which, is present to an extent of 7.7% compared to $^{12}C_7H_5^+$ in the beam; no adduct could be identified within this background limit. However, the experiment performed with perdeuterated benzene verified the formation of the C_7D_6 adduct since a signal at $m/e=96$ was detected (Figs. 7 and 8); the contribution of background signal of $^{13}C_2{}^{12}C_5D_5^+$ to $^{12}C_7D_6^+$ is marginal. We would like to stress that $m/e=96$ should fragment to $m/e=94$ in the detector, and that the $m/e=94$ data accumulated at this specific collision energy (21.4 kJ mol^{-1}) should be fit with two reaction channels, i.e., the formation of an adduct and the atomic deuterium loss pathway. Within our error limits we could superimpose two channels to fit our data, but the contribution of the adduct is actually very small (<1 %), and no change in the fit with or without the adduct pathway to $m/e=94$ was noticed (see also Sec. VIII B).

B. Laboratory angular distributions (LAB) and TOF spectra

The most probable Newton diagrams of the reaction $C(^3P_j)+C_6H_6(X\,^1A_{1g})\rightarrow C_7H_5+H(^2S_{1/2})$ together with the laboratory product angular (LAB) distributions and TOFs are shown in Figs. 1–6 at selected collision energies. All LAB distributions are very narrow (25°–30°) and peak close to the center-of-mass angles for collision energies less than 25 kJ mol^{-1}. As the collision energies increase, the maxima shift slightly in the backward directions toward the benzene beam. Assuming a delta function of the relative collision energy and no angular spread of the supersonic beams, we expect a single peak at the LAB distribution for the C_7D_6 adduct (Fig. 7). However, due to the velocity broadening and angular divergence of both beams, the actual data show a very narrow angular distribution over 10° within the scattering plane.

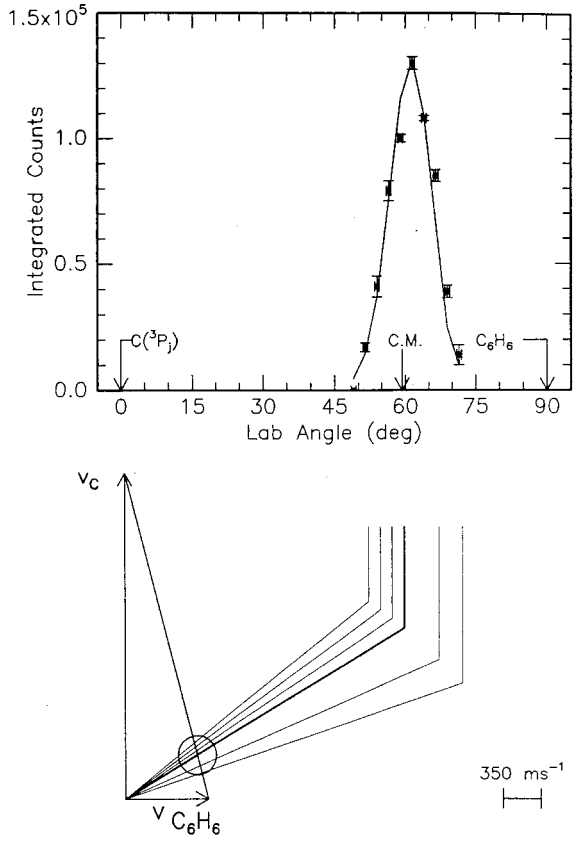

FIG. 3. Lower: Newton diagram for the reaction $C(^3P_j)+C_6H_6(X\,^1A_{1g}) \rightarrow C_7H_5+H(^2S_{1/2})$ at a collision energy of 50.3 kJ mol^{-1}. The circle stands for the maximum center-of-mass recoil velocity of the 1,2-didehydrocycloheptatrienyl product assuming all the available energy is released as translational energy. Upper: Laboratory angular distribution of the C_7H_5 product. Circles and error bars indicate experimental data, the solid line the best fit distribution.

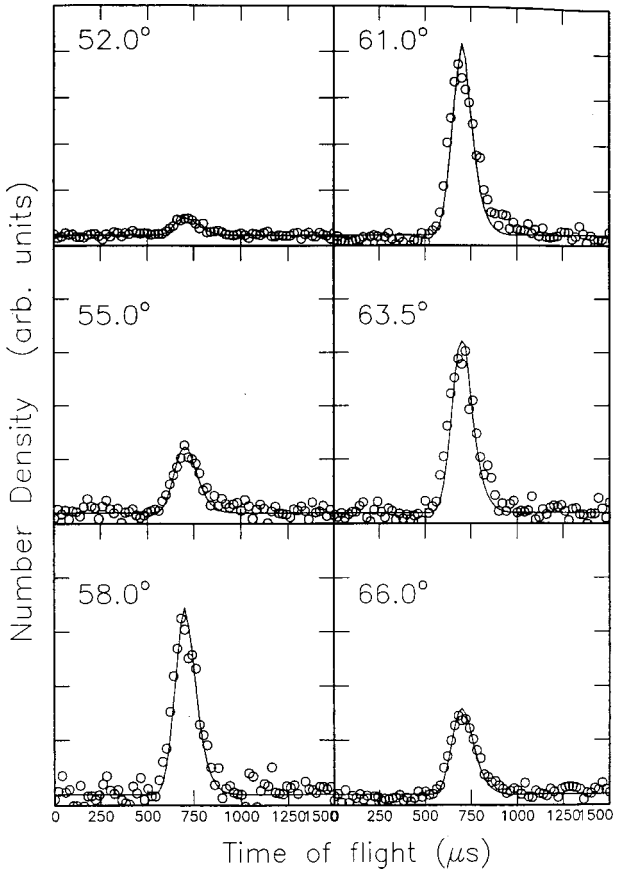

FIG. 4. Time-of-flight data of distinct laboratory angles as indicated in Fig. 1 for collision energy 17.0 kJ mol^{-1}. The dots indicate the experimental data, the solid lines the calculated, best fit curve.

C. Center-of-mass translational energy distributions, $P(E_T)$

Our data at $m/e=94\,(C_7D_5^+)$ and 89 $(C_7H_5^+)$ were fitted assuming that one single reaction channel is responsible for the observed LAB distributions and TOF spectra. The best-fit center-of-mass functions are presented in Figs. 9–11 for selected collision energies; all remaining data are compiled in the EPAPS database.[31] A thorough error analysis was performed, and all functions shown are within the upper and lower experimental error limits of the LAB data. The $P(E_T)$ for all twelve collision energies exhibit a similar shape and peak at zero translational energy. The energy maxima E_{max} of the distributions were found to increase as the collision energy rises, and the best-fit $P(E_T)$ show energy tails extending to (21, 35, 51, 58, 70) kJ mol^{-1} at the collision energies (8.8, 21.4, 32.1, 43.7, 52.5) kJ mol^{-1} of the C_6D_6 reaction as well as to (26, 45, 45, 47, 47, 59, 72) kJ mol^{-1} at (9.4, 17.0, 21.8, 26.9, 36.7, 41.1, 50.3) kJ mol^{-1} for the C_6H_6 reaction. This high-energy cutoff represents the sum of the reaction exothermicity plus the relative collision energy. Therefore, if we subtract the relative collision energy for each data set and average the results, the reactions are found to be exothermic by 12.2 ± 3.7 kJ mol^{-1} $[C(^3P_j)+C_6D_6(X\,^1A_{1g})\rightarrow C_7D_5+D(^2S_{1/2})]$ and 15.6 ± 4.8 kJ mol^{-1} $[C(^3P_j)+C_6H_6(X\,^1A_{1g})\rightarrow C_7H_5+H(^2S_{1/2})]$.

D. Center-of-mass angular distributions, $T(\theta)$

At lower collision energies, the $T(\theta)$ are forward–backward symmetric. This suggests that the chemical reaction dynamics are indirect and proceed through complex formation. The 0°–180° symmetry underlines further that the lifetime of the decomposing complex is longer than its rotational period. Alternatively, the fragmenting intermediate is symmetric. Here, a C_2 rotation axis might interconvert leaving hydrogen atoms in the C_7H_6/C_7D_6 complexes, and the complex would then fragment with equal probability in θ and $\pi-\theta$. These characteristics would result in a symmetric flux distribution even if the lifetime of the complex might be less than a rotational period.[32] The flat distributions indicate, further, that the initial ($\mathbf{L}$) and final ($\mathbf{L}'$) orbital angular momenta are poorly correlated, as a significant amount of total angular momentum $\mathbf{J}$ must channel into the rotational excitation $\mathbf{J}'$ of the reaction product.[33] This is the effect of the light mass of the leaving H and D atoms and hence their ineffectiveness to carry away a significant amount of final orbital angular momentum. As the collision energy increases, the shape of the $T(\theta)$ changes dramatically, showing an in-

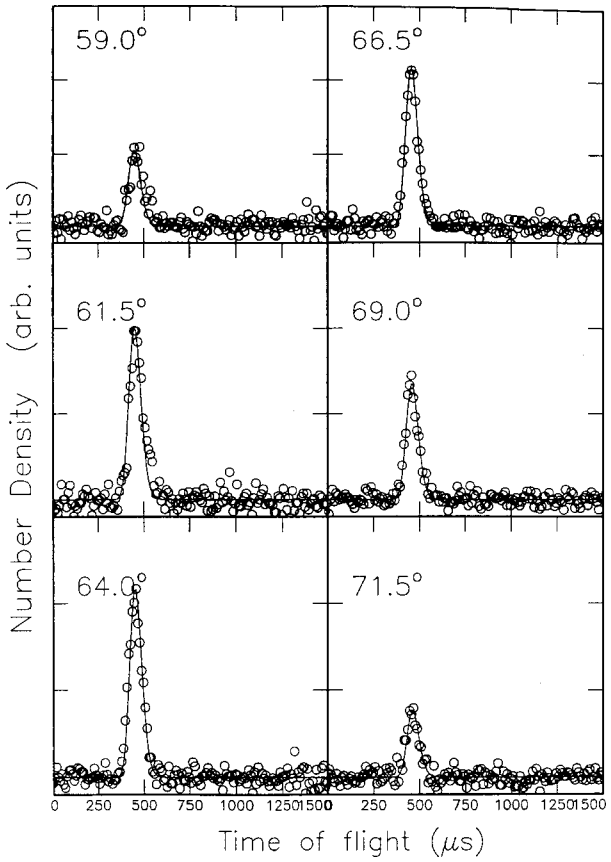

FIG. 5. Time-of-flight data of distinct laboratory angles as indicated in Fig. 2 for collision energy 36.7 kJ mol^{-1}. The dots indicate the experimental data, the solid lines the calculated, best-fit curve.

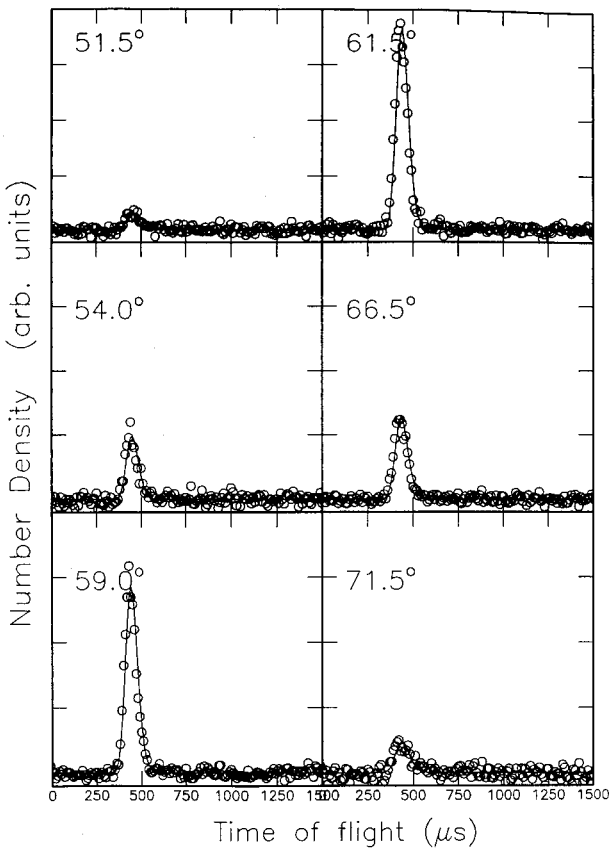

FIG. 6. Time-of-flight data of distinct laboratory angles as indicated in Fig. 3 for collision energy 50.3 kJ mol^{-1}. The dots indicate the experimental data, the solid lines the calculated, best-fit curve.

creased backward peaking with rising collision energy. Interestingly, the onset of this asymmetry differs for the benzene and perdeutero benzene systems and starts at about 32–43 kJ mol^{-1} (C_6D_6) and 27–37 kJ mol^{-1} (C_6H_6), respectively. This trend is visualized in Fig. 12 and suggests that at the same collision energy, the decomposing C_7D_6 complex might hold a longer lifetime than C_7H_6. Alternatively, these findings could account for two microchannels, i.e., an isotropic one (long-lived complex) at all collision energies and an additional backward-scattered contribution at higher collision energies. These options will be discussed in the following sections in the light of reactive impact parameters (see Sec. VIII C). We would like to stress that the enhanced backward peaking is neither a relic of the velocity spread of the beams nor the collision-energy-dependent variation of the relative cross section. Further, a thorough error analysis was performed, and all functions shown are within the upper and lower experimental error limits of the data.

VI. *AB INITIO* RESULTS

A. The H-atom loss channel

The pertinent part of the C_7H_6 potential energy surface has been studied previously by Bettinger *et al.*[15] at the B3LYP/6-311+G**+ZPVE(B3LYP/6-31G*) level of theory and is displayed in Fig. 13. To facilitate the discussion, we focus here on the computational results supporting our experiments and the RRKM investigations and refer the reader to Ref. 15 for more details concerning the PES. Briefly, the electrophilic carbon atom attacks benzene without a barrier and interacts with the π electron system to form a $^3A''$ C_s symmetric minimum **1T**; this is bound by 62 kJ mol^{-1} with respect to the separated reactants (Fig. 13). The initial collision complex is only metastable: **1T** ring opens via a low barrier of only 4 kJ mol^{-1} via **TS1** to triplet cycloheptatrienylidene **2T**, which resides in a deep potential energy well of 294 kJ mol^{-1}. The latter might undergo ISC to the singlet surface to give **2S**, which is connected to **1S** via an isomerization through **TS5**. Alternatively, the added carbon atom in **1T** can formally insert into the adjacent C–H single bond via **TS2** to form triplet phenylcarbene **3T**, which represents the lowest minimum on this part of the triplet C_7H_6 PES (-342 kJ mol^{-1}). The barrier of this process is significantly higher (>40 kJ mol^{-1}) compared to the ring opening of **1T** to **2T**. A hydrogen shift from **1T** to **4T** is unimportant due to its high barrier of 44 kJ mol^{-1} with respect to reactants. Finally, **1T** could undergo intersystem crossing (ISC) to the singlet surface yielding **1S**. Both **2T** and **3T** can isomerize to the bicyclic triplet intermediate **4T** with barriers (**TS3** and **TS4**) well below the energy of the reactants. **TS3** is 7.6 kJ mol^{-1} lower in energy than the one found previously and differs by the orientation of the migrating H atom with respect to the plane of the three membered ring being formed. A [1,2]-H shift to **5T** is an alternative reaction pathway of **4T**. Since this hydrogen migration

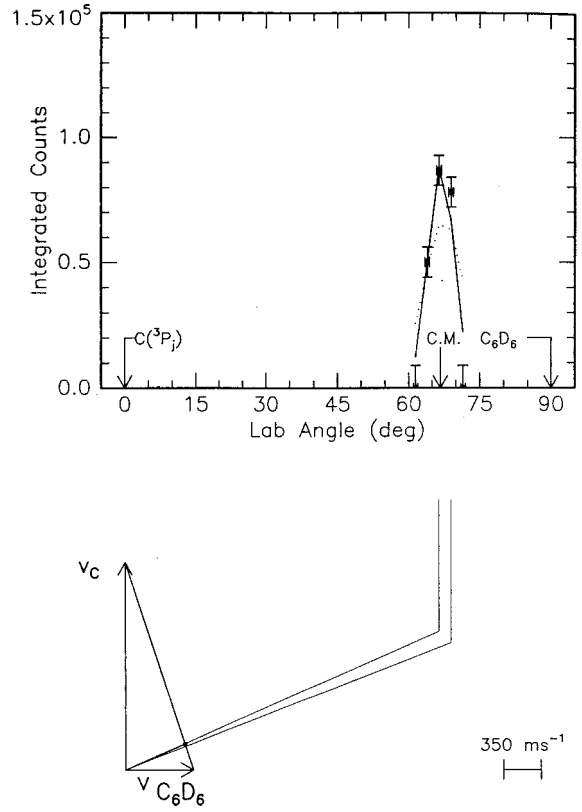

FIG. 7. Lower: Newton diagram for the reaction $C(^3P_j)+C_6D_6(X\,^1A_{1g}) \rightarrow C_7D_6$ at a collision energy of 21.4 kJ mol^{-1}. Upper: Laboratory angular distribution of the C_7D_6 adduct. Circles and error bars indicate experimental data, the solid line the calculated, best-fit distribution. Center-of-mass functions as obtained for $C(^3P_j)+C_6D_6(X\,^1A_{1g}) \rightarrow C_7D_5+D(^2S_{1/2})$ yielded a fit (dashed line) not superimposable with the experimental data.

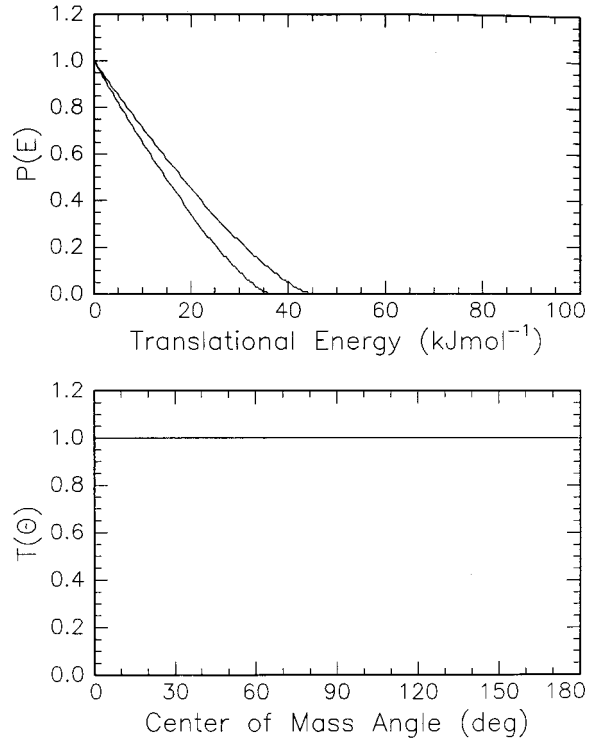

FIG. 9. Center-of-mass angular flux distribution (lower) and translational energy flux distribution (upper) for the reaction of $C(^3P_j)+C_6H_6(X\,^1A_{1g}) \rightarrow C_7H_5+H(^2S_{1/2})$ at a collision energy of 17.0 kJ mol^{-1}. The two lines correspond to the upper and lower error limits.

does not conserve orbital symmetry, the intrinsic barrier via **TS7** is significant (+155 kJ mol^{-1}), and the latter is located 15 kJ mol^{-1} above the separated reactants. The C_7H_6 intermediates can form two C_7H_5 products, the planar C_{2v} symmetric benzocyclopropenyl radical ($X\,^2B_1$) **p1** and the 1,2-didehydrocycloheptatrienyl radical ($X\,^2B_1$) **p2**, via a carbon–hydrogen bond rupture. First, **2T** and **2S** can emit a hydrogen atom adjacent to the ''inserted'' carbon atom without exit barriers to form **p2**. A second reaction pathway involves a decomposition of **4T** via a tight exit transition state **TS6** located 24 kJ mol^{-1} below the reactants to **p1**. The third reaction mechanism could involve a barrierless loss of a hydrogen atom from the methylene group of **5T** to yield **p1**. The overall reactions to **p1** and **p2** were found to be exothermic by 45 and 11 kJ mol^{-1}, respectively, at the B3LYP/6-311+G**+ZPVE(B3LYP/6-31G*) level of theory, while at the G2(B3LYP/MP2) level of theory, formation of **p2** was found to be exothermic by 7.9 kJ mol^{-1}.[15] Note that B3LYP and G2(B3LYP/MP2) underestimate the reaction exothermicity by 4 to 8 kJ mol^{-1} with respect to the experimentally deduced reaction exothermicity, whereas the ''complete basis set'' (CBS-Q) scheme[34] overestimates it by 10 kJ mol^{-1}.[15]

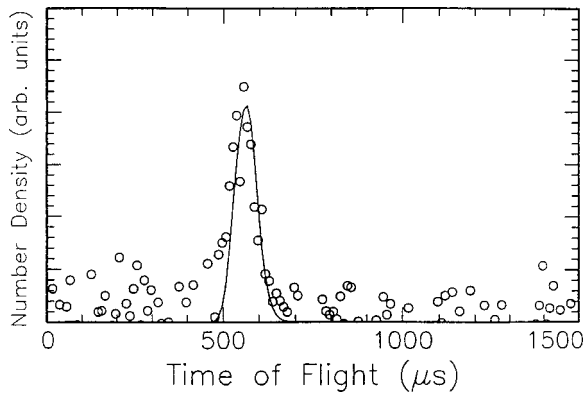

FIG. 8. Time-of-flight data of $m/e=96$ ($C_7D_6^+$) taken at the laboratory angle of 67° as indicated in Fig. 7 for collision energy 21.4 kJ mol^{-1}. The dots indicate the experimental data, the solid lines the calculated fit.

B. The H_2 loss channel

In the present paper, we investigate the $C_7H_4+H_2$ pathway as an alternative to H-atom loss. As both fragments have an even number of electrons, the reaction for the singlet electronic state is considered first, i.e., the H_2 elimination from cycloheptatetraene **2S**, cf. Fig. 14. No reaction pathway of any vicinal 1,2-H_2 elimination from **2S** could be located, and we thus investigate the energetics and transition state structures of a [1,2]-H atom shift in **2S** and a successive geminal 1,1-H_2 loss pathway.

The [1,2]-H shift of an allenic H atom in singlet cycloheptatetraene **2S** (C_2 symmetry) proceeds over a rather high barrier of 299 kJ mol^{-1} via **TS8**. Since singlet cycloheptatetraene is very low in energy compared to the reactants (−376 kJ mol^{-1}), this barrier can be surmounted without any

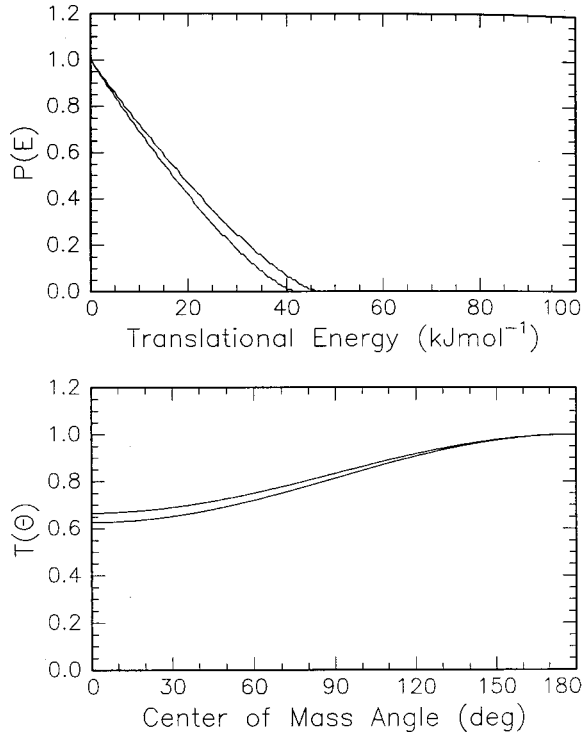

FIG. 10. Center-of-mass angular flux distribution (lower) and translational energy flux distribution (upper) for the reaction of $C(^3P_j)+C_6H_6(X\,^1A_{1g})\rightarrow C_7H_5+H(^2S_{1/2})$ at a collision energy of 36.7 kJ mol^{-1}. The two lines correspond to the upper and lower error limits.

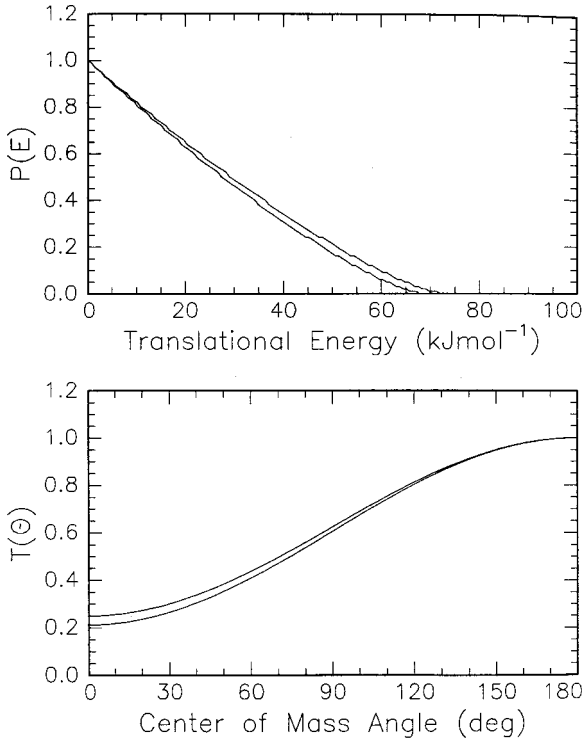

FIG. 11. Center-of-mass angular flux distribution (lower) and translational energy flux distribution (upper) for the reaction of $C(^3P_j)+C_6H_6(X\,^1A_{1g})\rightarrow C_7H_5+H(^2S_{1/2})$ at a collision energy of 50.3 kJ mol^{-1}. The two lines correspond to the upper and lower error limits.

additional energy. Note that the [1,2]-H shift in benzene to give cyclohexa-1,3-diene-5-ylidene has a significantly higher barrier of 374 kJ mol^{-1} at the CCSD(T)/DZP//B3LYP/DZP+ZPVE level of theory.[35] The product of the rearrangement is cyclohepta-1-yne-3,5-diene **(6S)**, the alkyne isomer of the allene. This cyclic alkyne is found to have C_s symmetry and is 82 kJ mol^{-1} higher in energy than the cyclic allene. Note that all current density functionals fail to give the relative stability of C_3H_4, allene and methylacetylene, correctly.[36] Experimentally, for example, methylacetylene is more stable by 12.5 kJ mol^{-1}, but B3LYP/6-311+G** favors allene by 6.7 kJ mol^{-1}. However, since the energy difference between the cyclic allene and the acetylene studied here is much larger than that of the C_3H_4 isomers, we do not expect the energetic ordering of isomers to change at higher levels of theory.

The barrier for H_2 elimination from **6S** via **TS9** is 311 kJ mol^{-1}; compared to the reactants, $C_6H_6+C(^3P)$, this process requires an additional energy of +16 kJ mol^{-1} [also 16 kJ mol^{-1} using the G2(B3LYP/MP2) approach]. The product of the H_2 elimination, formally the carbene, cyclohepta-1,3-diene-5-yne-7-ylidene, optimizes to a planar structure (C_{2v} symmetry cyclohepta-1,2,4,6-tetraene-1,3-diyl) (**p3S**). As B3LYP may not perform very well for such an electron-rich polydehydroannulene, we computed this isomer also using the multiconfigurational CASSCF method, where all configuration state functions (CSFs) obtained from the distribution of ten electrons into the seven π/π^* and three σ-allyl type orbitals were considered. The Hartree–Fock CSF clearly dominates the CASSCF wave function (coefficient $c_0=0.90$), followed by $c_1=-0.15$ and $c_2=0.10$. Six electrons occupy π orbitals, whereas four electrons occupy the bonding and nonbonding σ-allyl type orbitals of the C═C═C moiety. We also investigated the magnetic properties of **p3S** by computing the nuclear independent chemical shift (NICS)[37] in the center of the seven-membered ring [NICS(0)=−8.6] and 1.0 Å above the center of the ring [NICS(1)=−10.3] at the B3LYP/6-31G* level of theory.

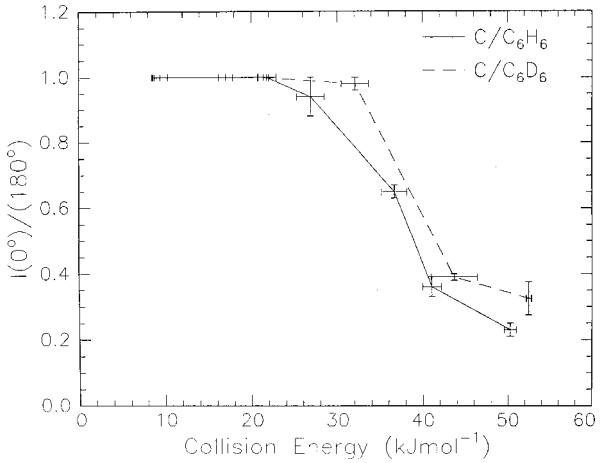

FIG. 12. Intensity ratios $I(0°)/I(180°)$ of the center-of-mass angular distributions for the reactions $C(^3P_j)+C_6H_6(X\,^1A_{1g})\rightarrow C_7H_5+H(^2S_{1/2})$ (solid line) and $C(^3P_j)+C_6D_6(X\,^1A_{1g})\rightarrow C_7D_5+D(^2S_{1/2})$ (dashed line) versus the collision energy.

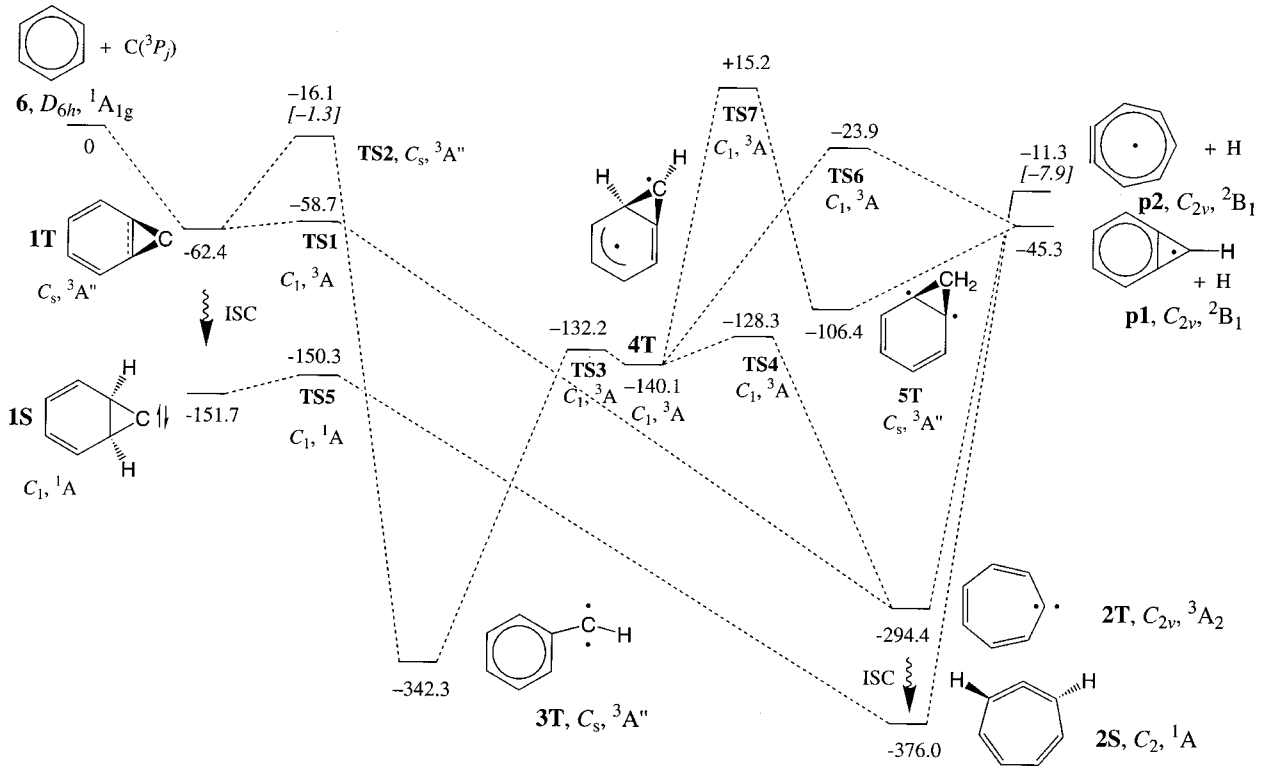

FIG. 13. Schematic representation of the C_7H_6 potential energy surface and reaction to two C_7H_5 isomers via atomic hydrogen loss as obtained in Ref. 15. Relative energies are given in kJ mol^{-1} and were computed at the B3LYP/6-311+G**+ZPVE(B3LYP/6-31G*) level of theory. The G2(B3LYP/MP2) data (where available) are given in brackets.

These values show that the six π electrons can sustain a diamagnetic ring current indicative of aromatic properties.

Although a detailed investigation of the C_7H_4 potential energy surface is beyond the scope of this paper, we nonetheless studied the electrocyclic ring closure of cyclohepta-1,2,3,4,6-tetraene-1-diyl to benzocyclopropenylidene (**p4S**). This reaction formally involves four electrons and is thus allowed in the Woodward–Hoffmann sense only if it proceeds conrotatorily.[38,39] We obtain a barrier 7 kJ mol^{-1} above the $C_6H_6+C(^3P)$ reactants for the formation of benzocyclopropenylidene. The latter is more stable than the cyclic cummulene by 63 kJ mol^{-1} at B3LYP/6-311+G**.

On the triplet PES a reaction mechanism analogous to that found on the singlet PES leads via hydrogen migration to triplet cyclohepta-1-yne-3,5-diene, **6T** (Fig. 15). Note that the energies of the transition state **TS11** and the intermediate are substantially higher than those of the corresponding singlet species throughout. Due to its open-shell character, **6T** preferentially eliminates an H atom to give the monocyclic C_7H_5 radical **p2** rather than an H_2 molecule. The reaction to the cyclohepta-1-yne-3,5-dienyl radical proceeds over a barrier (**TS12**) of +28 kJ mol^{-1} with respect to $C_6H_6+C(^3P_j)$. This reaction sequence is much less favorable than the C–H bond breaking in **2T**, which proceeds without a barrier. We therefore did not investigate the H_2 loss from triplet cyclohepta-1-yne-3,5-diene, as such a process needs, if it exists, to proceed through an electronically excited state, which is expected to be even higher in energy than the H-atom loss reaction.

C. Ring fragmentation

Finally, we consider the thermodynamics of exothermic reaction channels which involve the breaking of C–C bonds and therefore the fragmentation of the seven-membered ring. In our earlier work we found that the fragmentation into cyclopentadienylidene ($^3B_1$) and acetylene is exothermic by 56 kJ mol^{-1}.[15] Here, we also study the fragmentation to give $C_5H_2+C_2H_4$ (ethylene). Seburg *et al.*[40] identified the linear isomer as the lowest C_5H_2 radical at the coupled-cluster level including singles, doubles, and triples perturbatively in conjunction with a correlation consistent triple-ζ quality basis set [CCSD(T)/cc-pVTZ]. The ethynylcyclopropenylidene isomer is, however, only about 8 kJ mol^{-1} less stable. We find that the formation of $C_5H_2+C_2H_4$ is exothermic by 75 kJ mol^{-1} with respect to the reactants. Another possible outcome of a C_7H_6 fragmentation reaction is the generation of allene and diacetylene, HCCCCH, which is found to be exothermic by 170 kJ mol^{-1} with respect to the reactants.

It is clear that these molecules, formally accessible through highly exothermic reactions, cannot be produced from the monocyclic C_7H_6 isomers without going through energetically high-lying transition states. For example, consider the fragmentation of **2T** to cyclopentadienylidene ($^3B_1$) and acetylene. The cleavage of the ethenyl moiety from the cyclopentadienyl part needs to proceed over a barrier 16 kJ mol^{-1} above the separated reactants. Clearly, this process is more unfavorable than the simple C–H bond dissociation of the C_7H_6 intermediate which proceeds without barrier. We assume that the other exothermic ring frag-

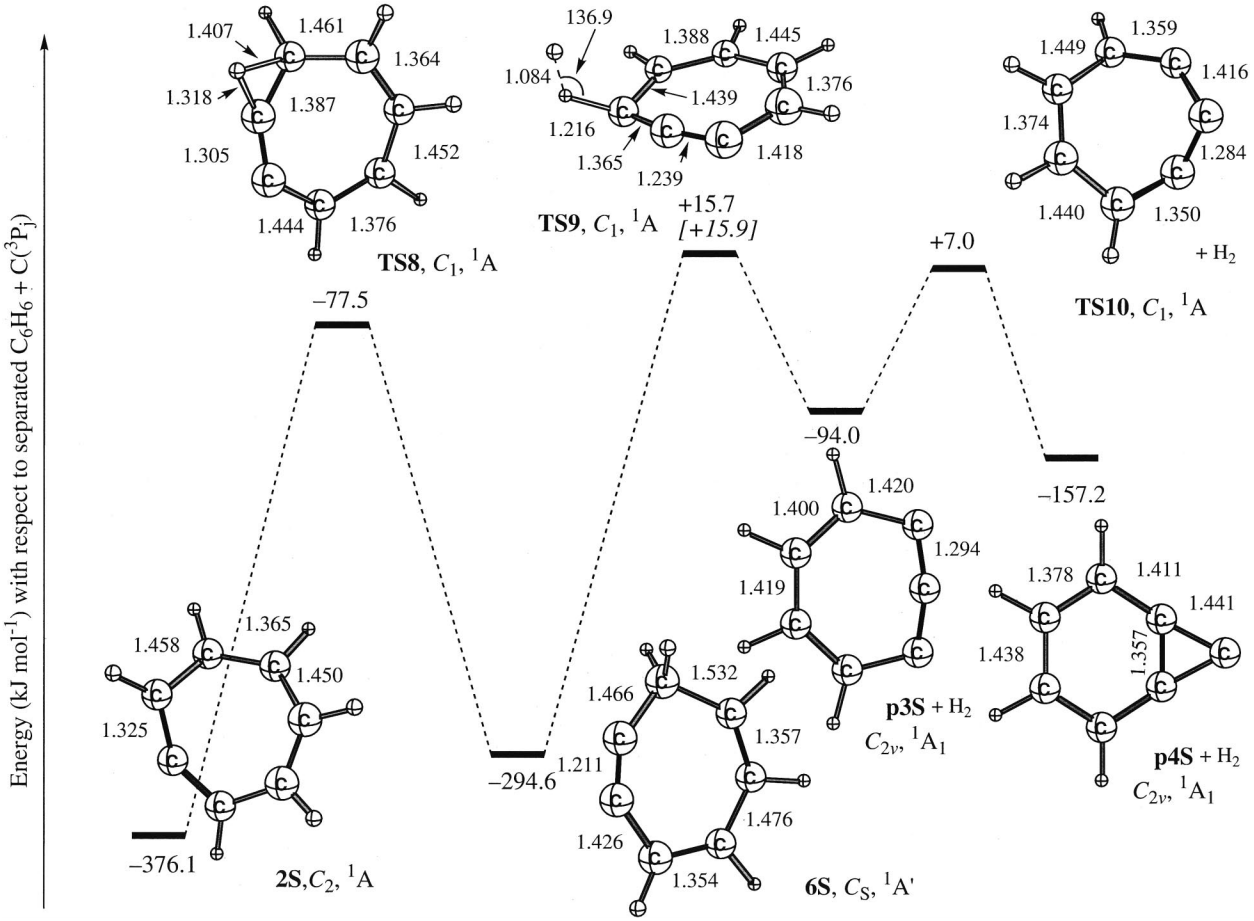

FIG. 14. Schematic representation of molecular hydrogen loss pathways on the singlet C_7H_6 potential energy surface to C_7H_4 isomers. Important bond distances are given in angstrom, bond angles in degrees. Energies [B3LYP/6-311+G**+ZPVE(B3LYP/6-31G*), kJ mol^{-1}] are presented with respect to the separated $C(^3P_j)$ and C_6H_6 reactants. Point groups and electronic wave functions are indicated as well. The G2(B3LYP/MP2) data (where available) are given in brackets.

mentation channels have similar, if not less favorable, energy requirements, and thus play only a minor role—if any—in the $C_6H_6+C(^3P_j)$ reaction studied under the single-collision conditions in a crossed molecular beams experiment.

D. Intersystem crossing

We consider two areas of the PES for intersystem crossing from the triplet to the singlet PES. First, we were able to locate a minimum on the seam of crossing between the $^3A''$ and $^1A'$ surfaces in the entrance channel. This surface hopping is due to the fact that the carbon atom prefers a triplet state for separated reactants, whereas the first stable triplet C_7H_6 complex formed (**1T**) is higher in energy than **1S**. The approximate spin–orbit coupling computation gives a norm of the spin–orbit coupling matrix element, $\langle H^{SO}\rangle$, of 17 cm^{-1}. The value of $\langle H^{SO}\rangle$ is known to converge slowly with the sizes of the CI and of the basis sets.[41] Hence, we have not attempted to improve upon the CASSCF(6,6)/6-31G* result, as the very short lifetime of **1T** given by the RRKM computations (see below), indicates that the ISC probability is small.

Cycloheptatrienylidene **2T** is another possible candidate for intersystem crossing. We earlier speculated that the lowest triplet state of **2T** might be $^3A_2$, whereas the singlet state energetically and geometrically closest to $^3A_2$–**2T** was found to be the planar $^1A_2$ state. As both states belong to the A_2 irreducible representation of the C_{2v} point group, and as the spin–orbit operator transforms as a rotation, the spin–orbit coupling between these states should be zero by symmetry.

VII. RRKM RESULTS

The theoretically obtained **p1**+H:**p2**+H product ratios in the low-pressure limit are very sensitive to the energy of the **p1**+H dissociation limit, and to the difference in energy between **TS6** and **p1**+H. Formation of **p1**+H through the reaction path **4T**→**TS7**→**5T**→**p1**+H (see Fig. 13) constitutes less than 1% of the **p1** formation; therefore this reaction path via **TS7** can be neglected. Given the difficulties encountered in the quantum-chemical calculation of the **p2**+H dissociation limit,[15] we opted to use the experimental value of -15.6 ± 4.6 kJ mol^{-1} relative to $C_6H_6+C(^3P_j)$. Using this value, we find that **p2** is the most important product with a yield of 76% at average energies of 60.4–120.8 kJ mol^{-1}, decreasing somewhat to 60% at 1.3 kJ mol^{-1}. We repeated our calculations using -20.1 kJ mol^{-1} for the **p2**+H dissociation limit, equal to the lower limit of the experimental value. We then find a nearly collision-energy independent

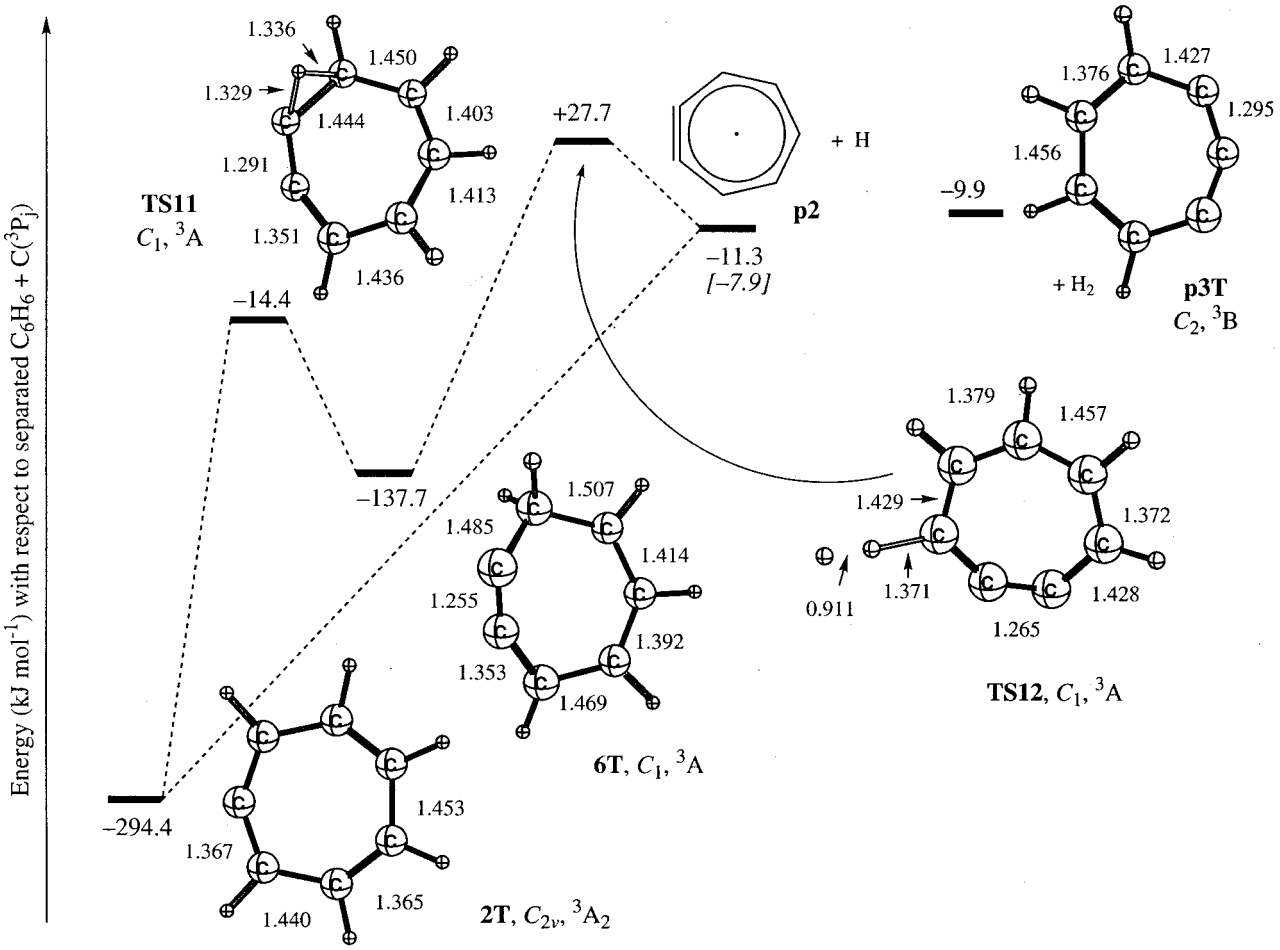

FIG. 15. Schematic representation of molecular hydrogen loss pathways on the triplet C_7H_6 potential energy surface to C_7H_4 isomers. Important bond distances are given in angstrom, bond angles in degrees. Energies [B3LYP/6-311+G**+ZPVE(B3LYP/6-31G*), kJ mol^{-1}] are presented with respect to the separated $C(^3P_j)$ and C_6H_6 reactants. Point groups and electronic wave functions are indicated as well.

p2+H:**p1**+H ratio of about 82:18. At this point, it is interesting to note that using the **p2**+H dissociation limit of −8 kJ mol^{-1} as calculated using the G2(B3LYP/MP2) method would result in **p2**+H:**p1**+H ratios of 11:89 at a collision energy of 1.3 kJ mol^{-1}, 28:72 at 60.4 kJ mol^{-1}, and 65:35 at 120.8 kJ mol^{-1}. The product distribution obtained is not sensitive to the estimated vibrational wave numbers for the entrance transition state, nor to the characteristics of the isomerization transition states **TS1**, **TS2**, **TS3**, or **TS4**. Redissociation of the chemically activated C_7H_6 adducts to $C_6H_6+C(^3P_j)$ is insignificant at low collision energies, but does affect the overall reaction rate constant if the collision energy increases, given that up to 30% of the C_7H_6 intermediates redissociate at an average collision energy of 120.8 kJ mol^{-1}.

An interesting consideration is the lifetime of the chemically activated triplet C_7H_6 intermediates in low-pressure conditions in view of a possible ISC from the triplet to the singlet C_7H_6 surface. Due to the low-lying transition state **TS1**, the lifetime of **1T**, about 10^{-12} s, is too short for significant intersystem crossing, leaving intermediate **2T** as the most likely candidate for ISC. Surface hopping in the gas phase will be mainly due to vibrational coupling between the triplet and singlet states. For averaged collision energies larger than 60.4 kJ mol^{-1}, the lifetime of **2T** is less than 250 μs, making ISC less probable. For lower energies, however, the lifetime of the C_7H_6 intermediates increases drastically, approaching 1 s before dissociation. Further studies of the surface-hopping rates are in order.

VIII. DISCUSSION

A. Identification of reaction product(s)—energetic constraints

Our experiments verify the existence of a carbon versus hydrogen (deuterium) exchange pathway to form C_7H_5 isomer(s) and their deuterated counterpart(s). The high-energy cutoffs of our $P(E_T)$ suggest the formation of the 1,2-didehydrocycloheptatrienyl radical, **p2**, in its $^2B_1$ electronic ground state. The experimental data give reaction exothermicities of 12.2±3.7 kJ mol^{-1} [$C(^3P_j)+C_6D_6(X\,^1A_{1g})$ reaction] and 15.6±4.8 kJ mol^{-1} [$C(^3P_j)+C_6H_6(X\,^1A_{1g})$ reaction], whereas B3LYP/6-311+G**+ZPVE(B3LYP/6-31G*) calculations yield 3 and 11 kJ mol^{-1}, respectively.[14,15] The formation of the more stable benzocyclopropenyl radical ($X\,^2B_1$), **p1**, is computed to be exothermic by 36 and 45 kJ mol^{-1} for the $C(^3P_j)/C_6D_6$ and $C(^3P_j)/C_6H_6$ systems, respectively, and hence this isomer can be excluded as a major

reaction product in the experiments. A detailed look at the pertinent potential energy surface supports these conclusions. Formation of **p1** can only proceed via **4T**; an alternative route through **5T** can be neglected since this process would pass through **TS7**. Since **TS7** was found to be 39 kJ mol^{-1} higher in energy than **TS6**, which leads to **p1**+H, **TS7** is expected to play no important role in the chemical reaction dynamics. This conclusion gains support from RRKM calculations, as formation of **p1** via **TS7** and **5T** accounts for less than 1% of **p1** formation. Therefore, a hydrogen loss via **TS6** located 24 kJ mol^{-1} below the separated products represents the only feasible reaction pathway to **p1**. However, due to this relatively tight exit transition state, we expect $P(E_T)$ distributions peaking well away from zero translational energy. This is clearly not found in our experiments, as the observed flux maxima at zero energy indicate a barrierless carbon–hydrogen bond cleavage. These characteristics were detected only for the decomposing complexes **2T** and **2S**. Besides the **p2** isomer, our experiments demonstrate the formation of an adduct C_7D_6, which will be discussed in Sec. VIII C.

B. Identification of reaction product(s)—RRKM studies

The theoretical predictions for the product distribution by RRKM—master equation analysis support the experimentally observed formation of **p2**+H as the most important product channel. The formation of the energetically more favorable **p1**+H product is estimated to be $\leqslant$20%. The predicted branching ratio is sufficiently sensitive to the energy of the **p2**+H dissociation limit to support the experimentally observed reaction exoergicity of -15.6 ± 4.8 kJ mol^{-1} as opposed to the quantum-chemical value of -7.9 kJ mol^{-1} obtained by G2(B3LYP/MP2).

Based on these RRKM calculations, the possible formation of **p1** was investigated more closely. Might the error limits of the $P(E_T)$, Figs. 9–11 and Ref. 31, account for a second, less-prominent reaction pathway to the thermodynamically favorable isomer **p1**? A second reaction channel was included in the parameter file, and the branching ratios of **p1** versus **p2** were optimized. This channel resulted in $P(E_T)$ peaking around 20–40 kJ mol^{-1} and reaction exothermicities from 40 to 60 kJ mol^{-1}. Therefore, the maximum contribution of **p1** is 10–15%, close to the RRKM result. However, this fit is superimposed based on our error limits; a one-channel fit without any contribution of **p1** could also fit our data satisfactorily. Clearly, more investigations are necessary to quantify the contribution of **p1** explicitly.

C. The actual reaction pathway

Based on the considerations above, the following chemical reaction dynamics are likely. C(^3P_j) attacks the benzene π–electron system without an entrance barrier to form an initial **1T** collision complex with two long carbon–carbon bonds (1.714 Å). Complex **1T** has C_s symmetry, a $^3A''$ electronic wave function, is bound by 62 kJ mol^{-1} with respect to the reactants, and undergoes ring opening to **2T**. An alternative insertion process via **TS2** to **3T** is not significant, as the inherent barrier lies $>$40 kJ mol^{-1} higher than **TS1**. Further, the lifetime of **1T** ranges around 10^{-12} s—too short for an ISC to **1S** on the singlet manifold to occur. Indeed, our experimental data suggest that the reaction proceeds solely on the triplet surface; see the discussion below. Therefore, we conclude that the ring opening **1T**$\rightarrow$**2T** is the dominating decay pathway. Since **1T** has C_s symmetry, the symmetry of the correlating $^3A_2$ electronic wave function of **2T** is reduced to $^3A''$.

But what is the fate of this **2T** complex? First, ISC to **2S** is unlikely. The spin–orbit coupling matrix elements from **2T** to **2S** ($^3A_2$ and $^1A_2$) vanish, making this process dipole forbidden. If **2S** existed, the molecular hydrogen loss channel via **2S**$\rightarrow$**6S**$\rightarrow$**p3S**+H_2 should have been observed in the experiments performed at higher collision energies. The exit barrier of 16.5 kJ mol^{-1} could have been overcome at nominal collision energies of 36.7, 41.1, and 50.3 kJ mol^{-1} in the C(^3P_j)/C_6H_6 system. Since TOFs and the laboratory angular distributions at $m/e=89$ ($C_7H_5^+$) and $m/e=88$ ($C_7H_4^+$) are fit with identical CM functions, the H_2 elimination channel, and hence ISC is expected to play only a minor role—if any—in the underlying chemical reaction dynamics. Moreover, no H_2 loss is anticipated on the triplet PES.

Rather than undergoing ISC, **2T** decomposes predominantly without an exit barrier to the thermodynamically less stable C_7H_5 isomer **p2**. The CM functions verify this reaction pathway: first, the experimentally determined reaction energies of -12.2 ± 3.7 kJ mol^{-1} [C(^3P_j)+C_6D_6($X\,^1A_{1g}$)] and -15.6 ± 4.8 kJ mol^{-1} [C(^3P_j)+C_6H_6($X\,^1A_{1g}$)] agree well with the theoretically computed values to form **p2** plus H and D, respectively (Sec. VIII A). Further, all $P(E_T)$ distributions peak at zero translational energy; this is expected for a C_7H_6 complex fragmenting without an exit barrier. Since the involvement of the singlet surface and hence **2S** can be excluded, only **2T** and **5T** can fragment without barrier to **p2**. Since formation of **5T** involves the reaction sequence **2T**$\rightarrow$**4T**$\rightarrow$**5T** and **TS7** is higher than **TS6**, **5T** is not likely to be formed. The RRKM calculations support this conclusion and indicate that the **4T**$\rightarrow$**TS7**$\rightarrow$**5T** reaction path contributes less than 1% to the production of **p1**+H. Thus, **2T** is clearly identified as the complex which decomposes into **p2**+H/D.

Besides the carbon versus hydrogen (deuterium) replacement channels, we observed the formation of a C_7D_6 adduct at a collision energy of 21.4 kJ mol^{-1} (Sec. V A). This adduct moves with a center-of-mass velocity of 800 m s^{-1}. Considering the flight length from the interaction region to the ionizer, C_7D_6 would need about 430 μs to reach the ionizer. For a collision energy of 21.4 kJ mol^{-1}, the RRKM lifetimes for all possible distributions of this excess energy over rotational and internal degrees of freedom are sufficiently long to allow a sizable fraction of the C_7D_6 intermediates to survive the flight to the ionizer, supporting the experimental detection of the C_7D_6 complex.

Finally, we address distinct attack geometries of the carbon atom towards the benzene molecule; see Figs. 16 and 17. This helps to understand the impact-parameter-dependent rotational excitation of the intermediates and the shape of the center-of-mass angular distributions. First, C(^3P_j) can ap-

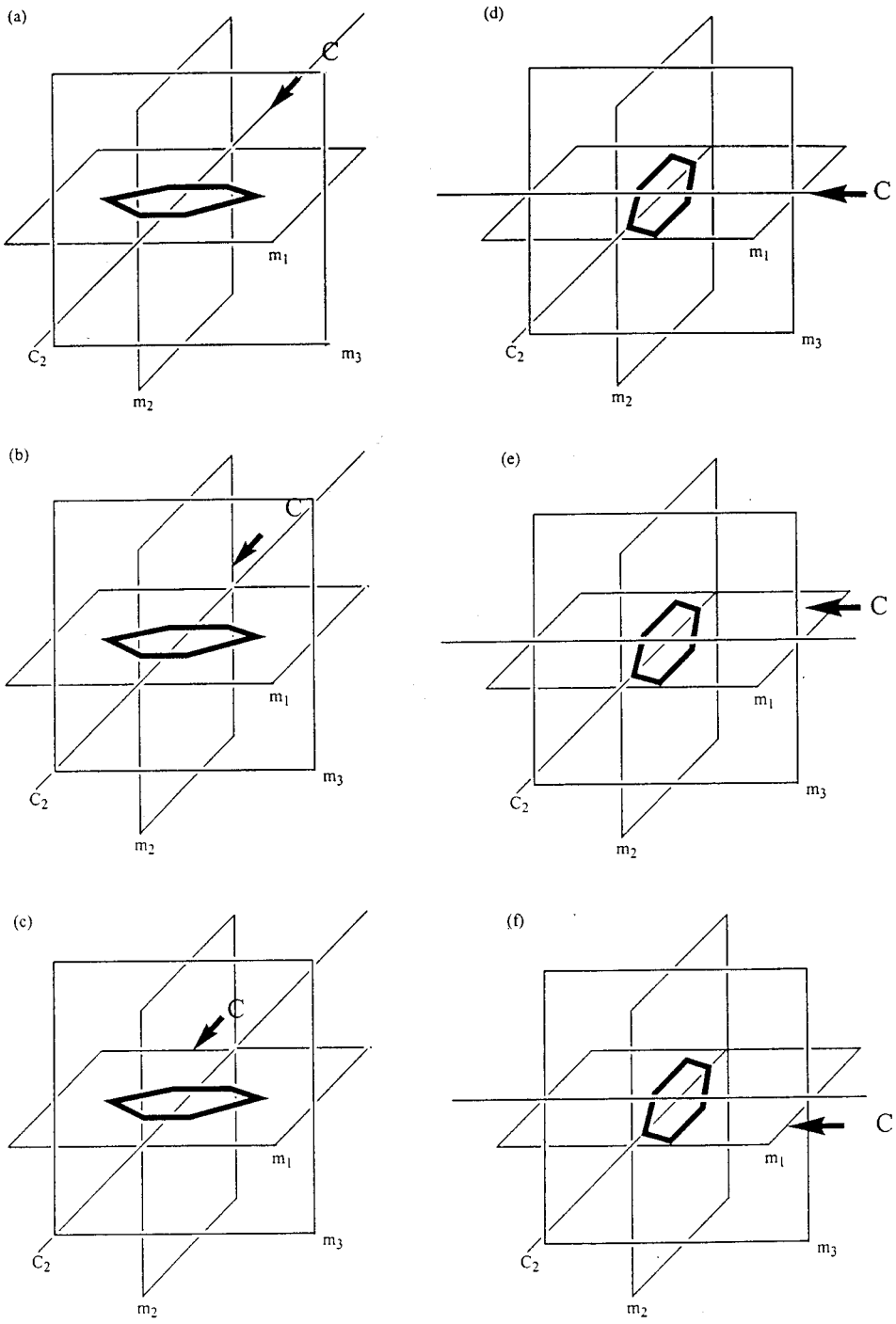

FIG. 16. Schematic approach geometries of $C(^3P_j)$ towards the benzene molecule.

proach the benzene ring edge-on [Figs. 16(a)–16(c)] or face-on [Figs. 16(d)–16(f)]. The edge-on or face-on types of approaches can lead, respectively, to preferential excitation of A [Fig. 16(b)], C [Fig. 16(c)], A [Fig. 16(e)], and B [Fig. 16(f)] rotations of the initial **1T** complex. Since such additions have no entrance barrier, the maximum impact parameter b is expected to decrease as the collision energy rises.[33] In the limit of $b=0$ Å, atomic carbon attacks the benzene ring either in the m_1 plane [Fig. 16(a)] or in the m_3 plane [Fig. 16(d)]. However, in-plane, edge-on trajectories in C_{2v} symmetry (a) are likely to be nonreactive, as two benzene hydrogen atoms inhibit such attacks sterically. Similar arguments suggest C_s trajectories (c) do not lead to reaction. Only the out-of-plane (b) carbon atom attack leads to favorable orbital overlap and hence reaction. On the other hand, the small impact parameters which follow edge-on trajectories could lead to reaction as orbital overlap is favorable, cf. Figs. 16(e) and 16(f). The closer the $C(^3P_j)$ attack is to the CM of benzene, the more backward-scattered the CM distribution should be. This was exactly the trend of an increasingly backward-scattering distribution was found with rising collision energy (and, hence, with a decreasing maximum impact parameter). These considerations suggest that the chemical dynamics is controlled by large impact parameters (barrierless reaction) at low collision energies, and that the reaction can proceed either via edge-on (b) or face-on (e)/(f)

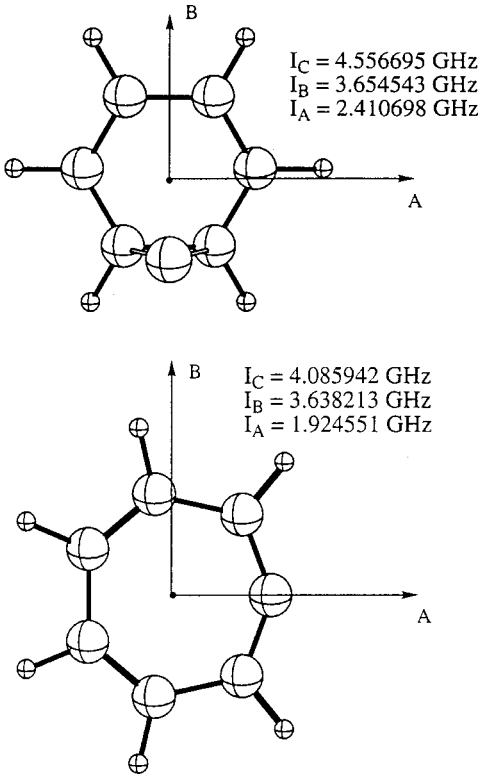

FIG. 17. Principal rotational axes of **1T** (top) and **2T** (bottom).

attacks of the benzene ring. Forward–backward symmetric $T(\theta)$ result. However, as the collision energy increases, the maximum impact parameter is reduced, and reactive collisions are suggested to proceed via smaller impact parameters closer to the CM of the benzene ring. These trajectories give rise to an enhanced backward-scattered contribution, i.e., a direct component of the reaction mechanism in which the C_7D_6/C_7H_6 intermediates are short-lived.[42]

D. Comparison with the $O(^3P_j)+C_6H_6$ reaction

The dynamics of the reaction of $O(^3P_j)$ with C_6H_6 and with C_6D_6 was studied in a previous crossed-beam experiment at two collision energies, 10.5 and 27.3 kJ mol^{-1},[11] and also very recently by quantum-chemical and RRKM theories.[43] Two major channels were detected experimentally. The oxygen atom was found to attack the aromatic ring to form an initial triplet biradial which subsequently decays by atomic hydrogen elimination to the phenoxy radical, C_6H_5O. At the higher collision energy a second channel was observed, and the triplet biradial was suggested to decay via nonradiative transition to the S_0 manifold of phenol. Although both atomic carbon and oxygen have ^3P configurations, their reactivity with benzene is remarkably different. First, no ring opening was found in the $O(^3P_j)/C_6D_6$ system, whereas a ring opening is the sole pathway for the isomerization of **1T** to **2T**. This finding can be attributed to topologically distinct PESs, as no bicyclic, oxygen-bearing complex was formed in the initial addition step. Second, an ISC to the singlet manifold is suggested to account for the C_6H_6O adduct formation, whereas the $C(^3P_j)/C_6D_6$ system adduct is likely to be formed on the triplet surface. As pointed out earlier, the very low 4 kJ mol^{-1} barrier involved in the ring opening process **1T**→**2T** results in an inherently fast rate constant with which ISC cannot compete.

IX. IMPLICATIONS FOR INTERSTELLAR CHEMISTRY AND COMBUSTION PROCESSES

Our combined experimental and theoretical investigations demonstrate explicitly that the reaction of atomic carbon with benzene proceeds without an entrance barrier and is exothermic. Since all further transition states are well below the energy of the separated reactants, this reaction may be of fundamental importance in the transformation of benzene even in the low-temperature environments of the interstellar medium (ISM, 10 K). Hence, even in these coldest molecular clouds, the six-membered benzene ring can be enlarged by reaction with carbon atoms. In contrast, benzene is resistant towards attack by atomic oxygen, as entrance barriers of 16.6–20.5 kJ mol^{-1} (Ref. 11) inhibit this reaction in low-temperature environments. Likewise, the reaction with atomic nitrogen, $N(^4S)$, also is expected to have an entrance barrier and cannot happen in cold molecular clouds. This underlines the special ability of atomic carbon to be incorporated into aromatic hydrocarbon molecules under expansion of the cyclic structure. As benzene represents the common ''building block'' of ubiquitous PAH-like species in the interstellar environments, our results suggest that atomic carbon might react with these molecules as well. The situation can be more diverse, since more complex PAHs not only contain benzenoid units but also possess ethylenic-like (C═C) and butadiene-like C═C–C═C moieties as found in phenanthrene and anthracene. However, the more complicated the astrophysically relevant molecular systems are, the more difficult experimental investigations become. Therefore, it is necessary to understand simple, prototype systems, e.g., the reaction of carbon atoms with benzene, to be able to develop versatile concepts first before attempting to unravel the chemical reactivity of more complicated molecules.

Even with unimolecular lifetimes approaching seconds, the collision frequency in the interstellar medium is still too low for a significant energy loss in the chemically activated C_7H_6 intermediates by collisional energy transfer via a third-body reaction. Formation of any stable C_7H_6 adduct will therefore never be important in the extremely low-pressure conditions of the ISM. Conversely, with regard to the reaction of atomic carbon with benzene in soot growth and atmospheric combustion systems, the RRKM results suggest that nearly all of the C_7H_6 intermediates will be thermalized collisionally, thus blocking dissociation to **p1**+H or **p2**+H. Using 1 atm of air as the bath gas, the stabilization rates are sufficiently high to prevent significant isomerization between **2T** and **3T**; thus, **2T** is the only product in atmospheric combustion systems for reactions proceeding via a long-lived intermediate. However, the crossed-beam experiments demonstrated explicitly that two micromechanisms exist, i.e., a complex-forming pathway at all collision energies, and an additional direct contribution at higher collision energies. The latter cannot be accounted for in our RRKM models, as such statistical-kinetics investigations do not in-

clude direct reaction channels. Therefore, we must conclude that C_7H_5 isomer(s) might be formed via a direct reaction pathway even in combustion processes.

X. CONCLUSIONS

The reaction of atomic carbon, $C(^3P_j)$, with benzene, $C_6H_6(X\,^1A_{1g})$, and with d_6-benzene $C_6D_6(X\,^1A_{1g})$, was investigated at 12 averaged collision energies between 8.8 and 52.5 kJ mol^{-1} using the crossed molecular beams technique. Forward-convolution fitting of the data was combined with high-level electronic structure calculations and RRKM investigations on the C_7D_6/C_7H_6 PESs. These investigations suggest that the chemical reaction dynamics are indirect and dominated by large reactive impact parameters. The reaction proceeds on the triplet surface via a barrierless addition of the carbon atom to form **1T**, followed by ring opening of the initial collision complex to **2T**. The latter was found to decompose without exit barrier to the thermodynamically less stable 1,2-didehydrocycloheptatrienyl radical, $C_7H_5(X\,^2B_1)$ (**p2**), and its deuterated counterpart. The C_7D_6 adduct was observed experimentally as a second reaction product. Possible minor contributions of the second, thermodynamically more stable **p1** isomer remain to be resolved.

ACKNOWLEDGMENTS

R.I.K. is indebted to the Deutsche Forschungsgemeinschaft (DFG) for a *Habilitation* fellowship. The experiments were supported by Academia Sinica (Taiwan) and Deutsche Forschungsgemeinschaft. After September 2000, R.I.K. acknowledges funding from University of York, United Kingdom. The research at the University of Georgia was supported by the U.S. Department of Energy, Office of Basic Energy Sciences, Division of Chemical Sciences, Fundamental Interactions Branch, Grant No. DOE-DE-FG02-97-ER. H.F.B. thanks Professor Sander and Professor Scuseria for support and the Fonds der Chemischen Industrie for a Liebig Fellowship. We thank Sarah Wilsey (Oxford) for help. This work was performed within the *International Astrophysics Network*.

[1] T. Allain, E. Sedlmayr, and S. Leach, Astron. Astrophys. **323**, 163 (1997).
[2] J. R. Heath and R. J. Saykally, Science **274**, 1480 (1996); H. W. Kroto and K. McKay, Nature (London) **331**, 328 (1988); C. Sagan *et al.*, Ap. J. **414**, 399 (1993).
[3] W. Weltner and R. J. VanZee, Chem. Rev. **89**, 1713 (1989).
[4] N. M. Marinov, M. J. Castaldi, C. F. Melius, and W. Tsang, Combust. Sci. Technol. **128**, 295 (1997).
[5] K. Siegmann and K. Sattler, J. Chem. Phys. **112**, 698 (2000); N. M. Marinov *et al.*, Combust. Sci. Technol. **116/117**, 211 (1996); N. M. Marinov *et al.*, Combust. Flame **114**, 192 (1998).
[6] *Handbook of Polycyclic Aromatic Hydrocarbons: Emission Sources and Recent Progress in Analytical Chemistry*, edited by A. Bjorseth and T. Ramdahl (Dekker, New York, 1985).
[7] J. Cernicharo *et al.*, Ap. J. **546**, L123 (2001).
[8] I. Cherchneff and J. R. Barker, Ap. J. **394**, 703 (1992); I. Cherchneff, J. R. Barker, and A. G. G. M. Tielens, Ap. J. **401**, 269 (1992).
[9] R. Terzieva and E. Herbst, Ap. J. **513**, 287 (1999); **501**, 207 (1998). R. P. A. Bettens and E. Herbst, Int. J. Mass Spectrom. Ion Processes **149/150**, 321 (1995); H. W. Kroto, J. R. Heath, S. C. O'Brien, R. F. Curl, and R. E. Smalley, Ap. J. **314**, 352 (1987).
[10] N. Balucani, O. Asvany, A. H. H. Chang, S. H. Lin, Y. T. Lee, R. I. Kaiser, H. F. Bettinger, P. v. R. Schleyer, and H. F. Schaefer, J. Chem. Phys. **111**, 7457 (1999).
[11] S. J. Sibener *et al.*, J. Chem. Phys. **72**, 4341 (1980).
[12] G. A. Brinkman, P. Kuipers, G. A. J. Leurs, and L. Lindner, Appl. Radiat. Isot. **42**, 1123 (1991).
[13] B. M. Armstrong, F. Zheng, and P. B. Shevlin, J. Am. Chem. Soc. **120**, 6007 (1998).
[14] R. I. Kaiser, I. Hahndorf, L. C. L. Huang, Y. T. Lee, H. F. Bettinger, P. v. R. Schleyer, H. F. Schaefer, and P. R. Schreiner, J. Chem. Phys. **111**, 7457 (1999).
[15] H. F. Bettinger, P. v. R. Schleyer, H. F. Schaefer III, P. R. Schreiner, R. I. Kaiser, and Y. T. Lee, J. Chem. Phys. **113**, 4250 (2000).
[16] Y. T. Lee, J. D. McDonald, P. R. LeBreton, and D. R. Herschbach, Rev. Sci. Instrum. **40**, 1402 (1969).
[17] R. I. Kaiser and A. G. Suits, Rev. Sci. Instrum. **66**, 5405 (1995).
[18] G. O. Brink, Rev. Sci. Instrum. **37**, 857 (1966).
[19] M. S. Weis, Ph.D. thesis, University of California, Berkeley (1986).
[20] A. D. Becke, J. Chem. Phys. **98**, 5648 (1993).
[21] C. Lee, W. Yang, and R. G. Parr, Phys. Rev. B **37**, 785 (1988).
[22] L. A. Curtiss, K. Raghavachari, and J. A. Pople, J. Chem. Phys. **98**, 1293 (1993).
[23] C. W. Bauschlicher and H. Partridge, J. Chem. Phys. **103**, 1788 (1995).
[24] M. J. Frisch *et al.*, GAUSSIAN 98, Revision A7, Gaussian, Inc., Pittsburgh, PA, 1998.
[25] M. J. Bearpark, M. A. Robb, and H. B. Schlegel, Chem. Phys. Lett. **223**, 269 (1994).
[26] S. Koseki, M. W. Schmidt, and M. S. Gordon, J. Phys. Chem. **96**, 10768 (1992).
[27] L. Vereecken, G. Huyberechts, and J. Peeters, J. Chem. Phys. **106**, 6564 (1997).
[28] W. Forst, *Theory of Unimolecular Reactions* (Academic New York, 1973); R. Gilbert and S. C. Smith, *Theory of Unimolecular and Recombination Reactions* (Blackwell Scientific, Oxford, 1990); K. Holbrook, M. Pilling, and S. Robertson, *Unimolecular Reactions*, 2nd ed. (Wiley, New York, 1996).
[29] L. Vereecken and J. Peeters, J. Phys. Chem. A **103**, 5523 (1999).
[30] J. Troe, J. Chem. Phys. **66**, 4745 (1997); *ibid.* **66**, 4758 (1997).
[31] See EPAPS Document No. E-JCPSA6-115-014147 for a comprehensive set of data. This document may be retrieved via the EPAPS homepage (http://www.aip.org/pubservers/epaps.html) or from ftp.aip.org in the directory /epaps/. See the EPAPS homepage for more information.
[32] R. I. Kaiser, C. Ochsenfeld, M. Head-Gordon, and Y. T. Lee, Science **274**, 1508 (1996).
[33] R. D. Levine and R. B. Bernstein, *Molecular Reaction Dynamics and Chemical Reactivity* (Oxford University Press, Oxford, 1987).
[34] J. W. Ochterski, G. A. Peterson, and J. Montgommery, J. Chem. Phys. **104**, 2598 (1996).
[35] H. F. Bettinger, P. R. Schreiner, P. v. R. Schleyer, and H. F. Schaefer, J. Am. Chem. Soc. **120**, 5741 (1998).
[36] L. Woodcock, P. R. Schreiner, and H. F. Schaefer (unpublished).
[37] P. v. R. Schleyer, C. Dransfeld, H. Jiao, and N. J. R. van Eikema Hommes, J. Am. Chem. Soc. **118**, 6317 (1996).
[38] R. K. Frost *et al.*, J. Am. Chem. Soc. **118**, 4451 (1996).
[39] R. B. Woodward and R. Hoffmann, Angew. Chem. Int. Ed. Engl. **8**, 781 (1996).
[40] R. A. Seburg, R. J. McMahon, J. F. Stanton, and J. Gauss, J. Am. Chem. Soc. **119**, 10838 (1997).
[41] Z. Havlas, J. W. Downing, and J. Michl, J. Phys. Chem. A **102**, 5681 (1998).
[42] If the reaction mechanism is direct, we should not expect a peaking of the center-of-mass translational energy distributions at zero kinetic energy, but rather away from zero. However, within the error limits we can achieve a nonzero peaking as well (see the Discussion section).
[43] D. Hodgson, H.-Y. Zhang, M. R. Nimlos, and J. T. McKinnon, J. Phys. Chem. A **105**, 4316 (2001).